PNAS RESEARCH ARTICLE | CELL BIOLOGY OPEN ACCESS

# The FBXW7–KMT2 axis in cancer-associated fibroblasts controls tumor growth via an epigenetic-paracrine mechanism

Lu Yin[a,1], Jiagui Zhang[a,1], Zhipeng Zhu[b], Xiaojuan Peng[c], Huiyin Lan[a], Alex Ayoub[d], Mingjia Tan[e], Bo Zhou[f], Yaohui He[g], Siyuan Wang[a], Yan Lu[h,ij], Wen Liu[g], Xiufang Xiong[a], Jing Huang[c], Yali Dou[k,l], Fengbiao Mao[b], and Yi Sun[a,i,m,n,o,2]

Affiliations are included on p. 12.

Edited by Vishva Dixit, Genentech Inc., South San Francisco, CA; received November 8, 2024; accepted February 21, 2025

**F-box and WD repeat domain-containing 7 (FBXW7) is a tumor suppressor that targets various oncoproteins for degradation, but its role in modulating cancer-associated fibroblasts (CAFs) in the tumor microenvironment remains elusive. Here, we report that FBXW7 expression is gradually downregulated in CAFs during the progression of human pancreatic and lung cancers. Mechanically, FBXW7 inhibits histone lysine methyltransferase 2 (KMT2) methyltransferase activity via retinoblastoma binding protein 5 (RbBP5) binding, whereas FBXW7 depletion abrogates the binding to activate KMT2, leading to increased H3K4 methylations and global upregulation of gene expression. Activation of the interleukin-17 (IL-17) signaling pathway triggers the secretion of cytokines and chemokines to promote migration, invasion, and sphere formation of lung cancer cells. Coinjection of Fbxw7-depleted mouse embryonic fibroblasts with cancer cells enhances in vivo tumor growth, demonstrating a paracrine effect. Hypoxia downregulates CAF FBXW7 via ETS proto-oncogene 1 (ETS1) to increase H3K4 methylation, whereas conditioned media from hypoxia-exposed CAFs promotes migration and invasion of pancreatic cancer cells, highlighting FBXW7's tumor-suppressing role through KMT2 inactivation.**

FBXW7 E3 ligase | methyltransferase | epigenetic regulation | IL-17 signaling pathway | paracrine effect

## Significance

While F-box and WD repeat domain-containing 7 (FBXW7) is a typical tumor suppressor, frequently inactivated in human cancers, it is unknown whether FBXW7 also acts as a tumor suppressor via targeting cancer-associated fibroblasts (CAFs) in tumor microenvironment (TME). We report here that FBXW7 is gradually downregulated in CAFs as the progression of human pancreatic and lung cancers. Hypoxia-mediated downregulation of FBXW7 in CAFs activates histone lysine methyltransferase 2 (KMT2) methyltransferase, and epigenetically increases the secretion of inflammatory signals to promote tumor cell migration via a paracrine mechanism.

The tumor microenvironment (TME) consists of tumor cells and various types of cells, including immune cells [e.g., T cells, macrophages, neutrophils, natural killer (NK) cells, and dendritic cells (DCs)], cancer-associatedfibroblasts (CAFs), endothelial cells, and pericytes among others (1). In the TME, cancer cells actively interact with noncancerous cells via paracrine signaling by secreted proteins (e.g., cytokines, chemokines, growth factors, and proteases) (2) to maintain a tumor-supportive environment, thus promoting tumorigenesis (1).

CAFs in the TME are major components of the stroma, which secrete growth factors, cytokines, chemokines, and extracellular matrix proteins, such as IL-6, CXCL1, CXCL12, and granulocyte-colony stimulating factor (G-CSF), to promote tumor progression (3, 4). Coinjection of CAFs with skin carcinoma cells significantly promotes the growth of cancer cells, suggesting a tumor-promoting function of CAFs in vivo (5). Currently, various CAF-targeting strategies such as extracellular matrix (ECM)-targeting agents, anti-immunosuppressive strategies, and pathway-specific inhibitors, have emerged in preclinical and clinical trials for anticancer applications (3). However, the mechanism by which epigenetic regulation within CAFs affects the secretion of inflammatory cytokines and chemokines remains elusive.

F-box and WD repeat domain-containing 7 (FBXW7) is a substrate receptor subunit of Cullin-RING ligase-1 (CRL1), also known as SCF (SKP1-Cullin1-F-box protein), composing of a scaffold protein Cullin-1, an adaptor protein SKP1, a RING component RBX1 or RBX2, and an F-box protein responsible for substrate recognition (6). Among the 69 F-box proteins encoded in the human genome, FBXW7 is one of the most well studied (7). The F-box domain of FBXW7 interacts with SKP1 to facilitate the assembly of the SCF complex, whereas its C-terminal WD40 domain recognizes and binds to its substrates to promote polyubiquitylation via the K48 linkage of its substrates for proteasomal degradation (7). Many FBXW7 substrates are classic oncogenic proteins such as c-MYC, NOTCH1, c-JUN, and MCL-1 (7, 8). Loss-of-function mutations of FBXW7 are frequently observed in human cancers, leading to the accumulation of oncoproteins that promote tumorigenesis (7, 8). Furthermore, our previous studies showed that FBXW7 could also facilitate nonhomologous end-joining via K63-linked polyubiquitylation of XRCC4 (9), and upon LSD1 binding, FBXW7 undergoes self-ubiquitylation and degradation as an oncogenic mechanism

Author contributions: L.Y., J.Z., and Y.S. designed research; L.Y., J.Z., X.P., H.L., M.T., S.W., and A.A. performed research; Z.Z., Y.L., W.L., B.Z., and F.M. contributed new reagents/analytic tools; L.Y., J.Z., Z.Z., X.P., Y.H., W.L., X.X., J.H., Y.D., F.M., and Y.S. analyzed data; and L.Y. and Y.S. wrote the paper.

The authors declare no competing interest.

This article is a PNAS Direct Submission.



[1]L.Y. and J.Z. contributed equally to this work.

[2]To whom correspondence may be addressed. Email: yisun@zju.edu.cn.

This article contains supporting information online at https://www.pnas.org/lookup/suppl/doi:10.1073/pnas.2423130122/-/DCSupplemental.

Published March 24, 2025.

of LSD1 (10). In addition, FBXW7 has been shown to play a role in the inflammatory response. In a murine model of colitis, macrophage Fbxw7 promoted inflammation by increasing the expression of Ccl2 and Ccl7 (11), whereas FBXW7 in DCs also promoted inflammation by enhancing IL-23 expression (12). However, it is unknown whether and how FBXW7 regulates inflammation in CAFs of the TME to act as a tumor suppressor.

The histone lysine methyltransferase 2 (KMT2) family is highly conserved in eukaryotes, with six members: KMT2A, also known as mixed lineage leukemia-1 (MLL1), KMT2B, KMT2C, KMT2D, KMT2F, and KMT2G (13). They all contain a catalytic Su(var)3-9, enhancer-of-zeste and trithorax (SET) domain at the C-terminus that confers H3K4 methylation (14). KMT2 proteins reside in multisubunit complexes to achieve optimal enzymatic activity (13). The KMT2 core complex components include RbBP5 (Retinoblastoma binding protein 5), WD repeat protein 5 (WDR5), Absent, small, homeotic disks-2-like (ASH2L), and DumPY protein 30 (DPY30) (15, 16), and depletion of any of these subunits results in reduction of KMT2 activity and overall H3K4 methylation in vitro and in cells (17–19).

Histone H3K4 methylation, catalyzed by KMT2 family, is highly enriched at the promoters and enhancers of target genes, which is positively associated with high chromatin accessibility and transcription activation (13). Mutations in KMT2 family members are frequently found in various types of cancers, and among these, KMT2A is one of the most extensively studied, with chromosomal translocation in a significant subset of acute leukemia (20). Inactivation mutations of KMT2D were also been identified in different types of human tumors (21, 22). Furthermore, overexpression of KMT2A and KMT2D has been implicated in tumors with gain-of-function mutations of p53, resulting in a genome-wide increase of histone H3K4 methylation to promote proliferation of breast cancer cells (23). However, it is unknown whether and how FBXW7 interacts with KMT2 in the TME of pancreatic and lung cancers, and its biological consequences.

In this study, we report that FBXW7 serves as a tumor suppressor in CAFs, and its expression progressively decreases as the disease advances in human pancreatic and lung cancers. Mechanically, FBXW7 directly binds to RbBP5 to inactivate KMT2, whereas FBXW7 depletion markedly increases H3K4 methylations and activates the IL-17 signal, which promotes migration, invasion, and sphere formation in lung cancer cells in vitro and promotes tumor growth in vivo. Finally, hypoxia in the TME downregulates FBXW7 via ETS1 induction in pancreatic cancer-derived CAFs to trigger H3K4 methylations and promote the migration and invasion of pancreatic cancer cells. Collectively, FBXW7 acts as a tumor suppressor in CAFs in a paracrine manner by inactivating KMT2.

## Results

**FBXW7 Expression in CAFs Is Progressively Decreased As the Diseases Advance in Pancreatic and Lung Cancer Tissues.** Previous studies of FBXW7 as a tumor suppressor have mainly focused on in situ tumor cells per se. To investigate the potential role of FBXW7 in regulating the TME, an in-depth analysis of single-cell transcriptome datasets from PubMed was conducted in tissues from pancreatic cancer (24, 25) and lung cancer (26, 27). Using uniform manifold approximation and projection (UMAP) visualization, the cell populations in pancreatic cancer tissues were delineated into nine distinct clusters with annotations based on specifically expressed genes and canonical markers (Fig. 1*A* and *SI Appendix*, Fig. S1*A*). Among these clusters, T_NK was subdivided into four subclusters: $CD4^+$T, $CD8^+$T, NK, and Treg (Fig. 1*A*). Subsequent analysis of FBXW7 messenger RNA (mRNA) expression across different clinical stages revealed a progressive downregulation in FBXW7 mRNA, specifically in CAFs, as the disease progressed to more malignant stages in pancreatic cancer (Fig. 1*B*). In contrast, FBXW7 mRNA expression in pancreatic cancer tissues from other cell clusters, including epithelial, $CD4^+$T, $CD8^+$T, NK, Treg, myeloid, endothelial, B_plasma, and erythroid cells, showed relatively irregular trends as the disease progressed (Fig. 1 *C–H* and *SI Appendix*, Fig. S1 *C–G*). We further analyzed lung cancer tissues, where UMAP visualization identified seven distinct cell clusters annotated based on gene expression profiles and canonical markers (Fig. 1*I* and *SI Appendix*, Fig. S1*B*). Similarly, downregulation of FBXW7 mRNA was noted in CAFs as the disease progressed to more advanced stages (Fig. 1*J*), whereas other cell clusters again exhibited irregular trends, independent of the disease stages (Fig. 1 *K–P* and *SI Appendix*, Fig. S1 *H–J*). Collectively, progressive downregulation, as diseases advanced, of FBXW7 in CAFs suggests that CAF FBXW7 could play a tumor-suppressive role in the progression of human pancreatic and lung cancers.

**FBXW7 Directly Interacts with RbBP5 in the KMT2 Complex.** Since FBXW7 is progressively reduced in CAFs within the TME of the pancreatic and lung cancers as the disease progresses, we hypothesized that CAFs with downregulated FBXW7 would promote the growth of nearby tumor cells in a paracrine fashion. Given FBXW7 is not a transcription factor, we further hypothesized that secretory factors, such as cytokines and chemokines, whose expression is subjected to epigenetic regulation upon FBXW7 downregulation, would play a major role in this process. To this end, we performed immunoprecipitation (IP)-based pulldown, followed by mass spectrometry analysis in HEK293 cells expressing 3xFLAG-FBXW7 to unbiasedly identify FBXW7 binding proteins with a focus on epigenetic regulators (*SI Appendix*, Fig. S2*A*). Among 194 FBXW7 binding candidates (*SI Appendix*, Table S1), six members of the KMT2 complex, including UTX, KMT2D, ASH2L, RbBP5, PTIP, and WDR5, were detected, in addition to SCF components CUL1 and SKP1, serving as internal positive controls (Fig. 2*A*).

We next attempted to confirm FBXW7 binding to most of these KMT2 components in multiple cell lines, including HEK293 (Fig. 2*B*), HCT116 colon cancer, and H1299 lung cancer cells (*SI Appendix*, Fig. S2 *B* and *C*). While FBXW7 binding to these components was cell line-dependent (note that FBXW7 binding to WDR5 and PTIP was not confirmed in HEK293 cells likely due to different sensitivity between two assays), FBXW7–RbBP5 binding was detected in all the lines tested (Fig. 2*B* and *SI Appendix*, Fig. S2 *B* and *C*). We further confirmed that under physiological conditions, endogenous FBXW7 binds to endogenous RbBP5 in human cancer cell lines (Fig. 2*C* and *SI Appendix*, Fig. S2*D*), as well as in mouse embryonic fibroblasts (MEFs) (Fig. 2*D*). Furthermore, an in vitro pull-down assay with recombinant proteins confirmed the direct binding of FBXW7 to RbBP5, but not with ASH2L or WDR5 (Fig. 2*E*). Finally, FBXW7 and RbBP5 colocalized in the nucleus in both HCT116 and H1299 cells (Fig. 2*F* and *SI Appendix*, Fig. S2*E*).

Next, we mapped the interaction domains in both FBXW7 and RbBP5 by ectopically expressing truncation mutants (Fig. 2*G*) to pull down endogenous partners in HEK293 and HCT116 cells. Both the N-terminal fragment (ΔWD40) and C-terminal fragment (WD40) of FBXW7 bind to RbBP5 (*SI Appendix*, Fig. S2 *F* and *G*), whereas only the N terminus of RbBP5 (AA 1-344) binds to FBXW7 (*SI Appendix*, Fig. S2*H*). We further examined the binding domain of RbBP5 with either the ΔWD40 or WD40 domain of FBXW7, and obtained similar results with the full-length FBXW7 (*SI Appendix*, Fig. S3 *A* and *B*). Collectively, FBXW7 appears to bind to RbBP5 directly via either the ΔWD40 or the WD40 domain, whereas the N-terminus of RbBP5 binds to FBXW7 (Fig. 2*G*).

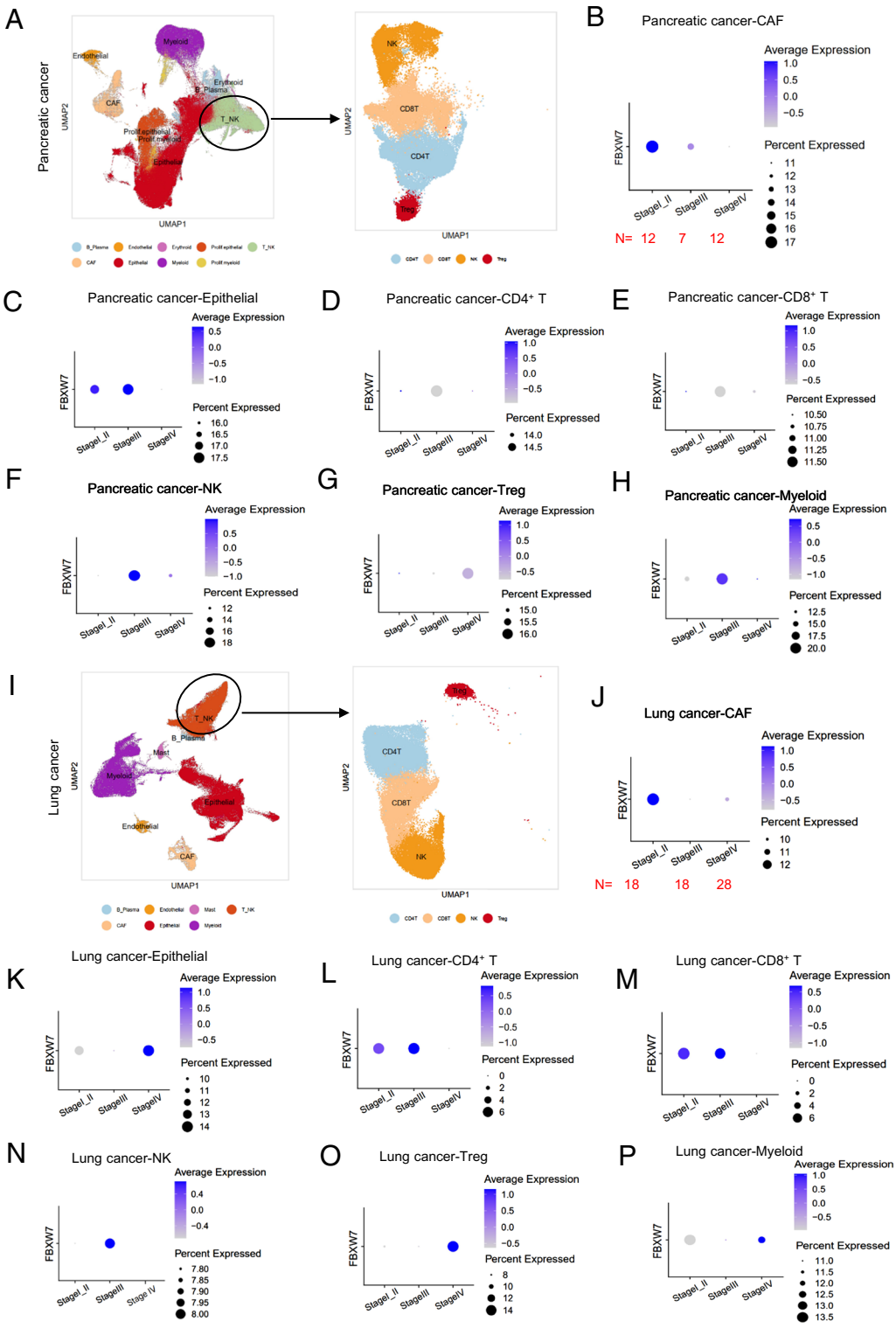


**Fig. 1.** FBXW7 expression in CAFs is progressively decreased as the diseases advance in pancreatic and lung cancer tissues. (*A*) UMAP visualization of the cell populations colored by annotated cell types in pancreatic cancer tissues. (*B–H*) Bubble charts show FBXW7 expression levels in pancreatic cancer tissues across different clinical stages in CAF (*B*), Epithelial (*C*) CD4$^+$T (*D*), CD8$^+$T (*E*), NK (*F*), Treg (*G*), and myeloid (*H*). (*I*) UMAP visualization of the cell populations colored by annotated cell types in lung cancer tissues. (*J–P*) Bubble charts show FBXW7 expression levels in lung cancer tissues across different clinical stages in CAF (*J*), Epithelial (*K*), CD4$^+$T (*L*), CD8$^+$T (*M*), NK (*N*), Treg (*O*), and myeloid (*P*).

**FBXW7 Does Not Destabilize RbBP5, but Competitively Inhibits RbBP5 Binding to Other KMT2 Components.** Next, we determined whether RbBP5 is a substrate of FBXW7. We first treated cells with MLN4924, a small molecule inhibitor of the neddylation activating enzyme, which inactivates CRL E3 ligases by blocking Cullin neddylation (28). MLN4924 had no effect on the protein level of RbBP5, but caused accumulation of NOTCH1 or c-JUN, two well-known substrates of FBXW7, serving as the positive controls (*SI Appendix*, Fig. S3 *C* and *D*). We next used HCT116 cells with or without *FBXW7* deletion and found that the levels of RbBP5, WDR5, ASH2L, and UTX remained unchanged, whereas the FBXW7 substrate c-MYC accumulated in FBXW7-null cells (Fig. 3*A*). The unchanged WDR5 level was inconsistent with a recent report (29).

Since a previous study showed that FBXW7 promotes KMT2D ubiquitylation and degradation in diffuse large B cell lymphoma cells (30), we also tested KMT2D levels upon FBXW7 silencing. Similarly, siRNA-mediated FBXW7 knockdown had no effect on RbBP5 and WDR5 levels in the two lung cancer cell lines (Fig. 3*B* and *SI Appendix*, Fig. S3*E*), nor did it affect KMT2D levels (Fig. 3 *A* and *B*). The RbBP5 protein level was also unaffected by FBXW7 overexpression at various doses (Fig. 3*C*). Finally, the protein

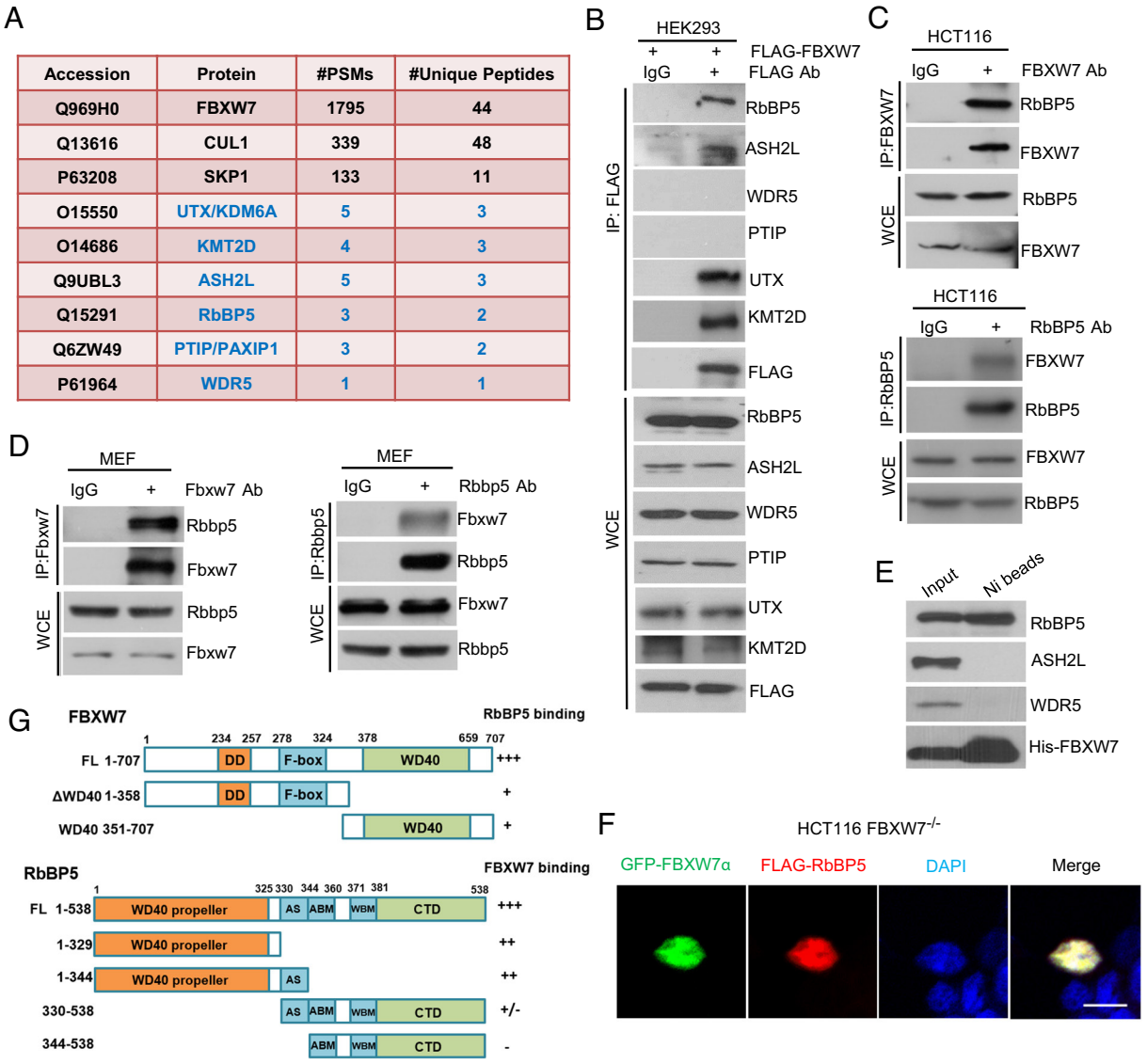


**Fig. 2.** FBXW7 directly interacts with RbBP5 in the KMT2 complex. (*A*) Six members of the KMT2 complex were identified as potential FBXW7 binding proteins by mass spectrometry. (*B*) HEK293 cells were transfected with FLAG-FBXW7, followed by IP with FLAG and immunoblotting (IB). WCE: whole cell extracts. (*C* and *D*) HCT116 (*C*) and MEFs (*D*) were harvested for IP with FBXW7 or RbBP5 Ab, along with normal IgG, followed by IB analysis. (*E*) Purified proteins were added to the reaction system, followed by pull-down with Ni beads and IB analysis. (*F*) HCT116 FBXW7$^{-/-}$ cells were cotransfected with green fluorescent protein (GFP)-FBXW7α and FLAG-RbBP5 for 48 h and then stained with FLAG Ab, followed by photography under a fluorescence microscope. (Scale bar: 10 μm.) (*G*) Truncated mutants of FBXW7 and RbBP5. FBXW7: (DD: dimerization domain; F-box: SKP1 binding region; WD40: substrate recognition and binding region); RbBP5: (WD40 propeller: consisting of seven repeats of the WD40 propeller; AS: activation segment; ABM: ASH2L-binding motif; WBM: WDR5-binding motif; CTD: C-terminal distal domain).

half-life of RbBP5, as well as other KMT2 components, including WDR5, ASH2L, PTIP, and UTX, were not affected by FBXW7 overexpression or deletion/depletion in two human cancer cell lines (*SI Appendix*, Fig. S3 *F–J*). Taken together, these results clearly demonstrate that FBXW7 does not destabilize RbBP5 or the other KMT2 components that we examined.

Since the WD40 propeller domain and activation segment (AS) of RbBP5 are important for the activity of the KMT2 complex (31), we next determined whether the FBXW7–RbBP5 interaction interferes with the RbBP5–KMT2 interaction. Indeed, FBXW7 overexpression reduced RbBP5 interaction with KMT2A or KMT2F in a dose-dependent manner, but did not affect binding to other components (Fig. 3*D*). On the other hand, FBXW7 knockdown in HEK293 cells, or Fbxw7 depletion in MEFs, enhanced the binding between RbBP5 and KMT2A, KMT2F, PTIP in human cells, or Kmt2a, Kmt2f, Ptip, Wdr5 in mouse cells, respectively, but in a cell line-dependent manner (Fig. 3 *E* and *F*). These results suggest that FBXW7 acts by competitively inhibiting the binding of RbBP5 to the KMT2 complex.

**FBXW7 Inhibits KMT2 Methyltransferase Activity.** RbBP5 is essential for the KMT2 enzymatic activities (15, 16). Given that FBXW7 interferes with RbBP5 binding to the KMT2 complex, we first tested whether FBXW7 affects the methyltransferase activity of KMT2 on histone H3 Lys4 (H3K4). Indeed, FBXW7 knockdown significantly increased the levels of mono-, di-, and tri-methylation of H3K4 (H3K4me1, H3K4me2, and H3K4me3) in HEK293 (Fig. 4*A*), H1299 (*SI Appendix*, Fig. S4*A*), and HeLa cells (*SI Appendix*, Fig. S4*B*). Likewise, genetic deletion of *FBXW7* increased the levels of H3K4me1, H3K4me2, and H3K4me3 in HCT116 cells (Fig. 4*B*) and MEFs (Fig. 4*C*).

For our subsequent in vivo study, we used immortalized MEFs induced by p53 deletion. To exclude the possible effect of p53 on

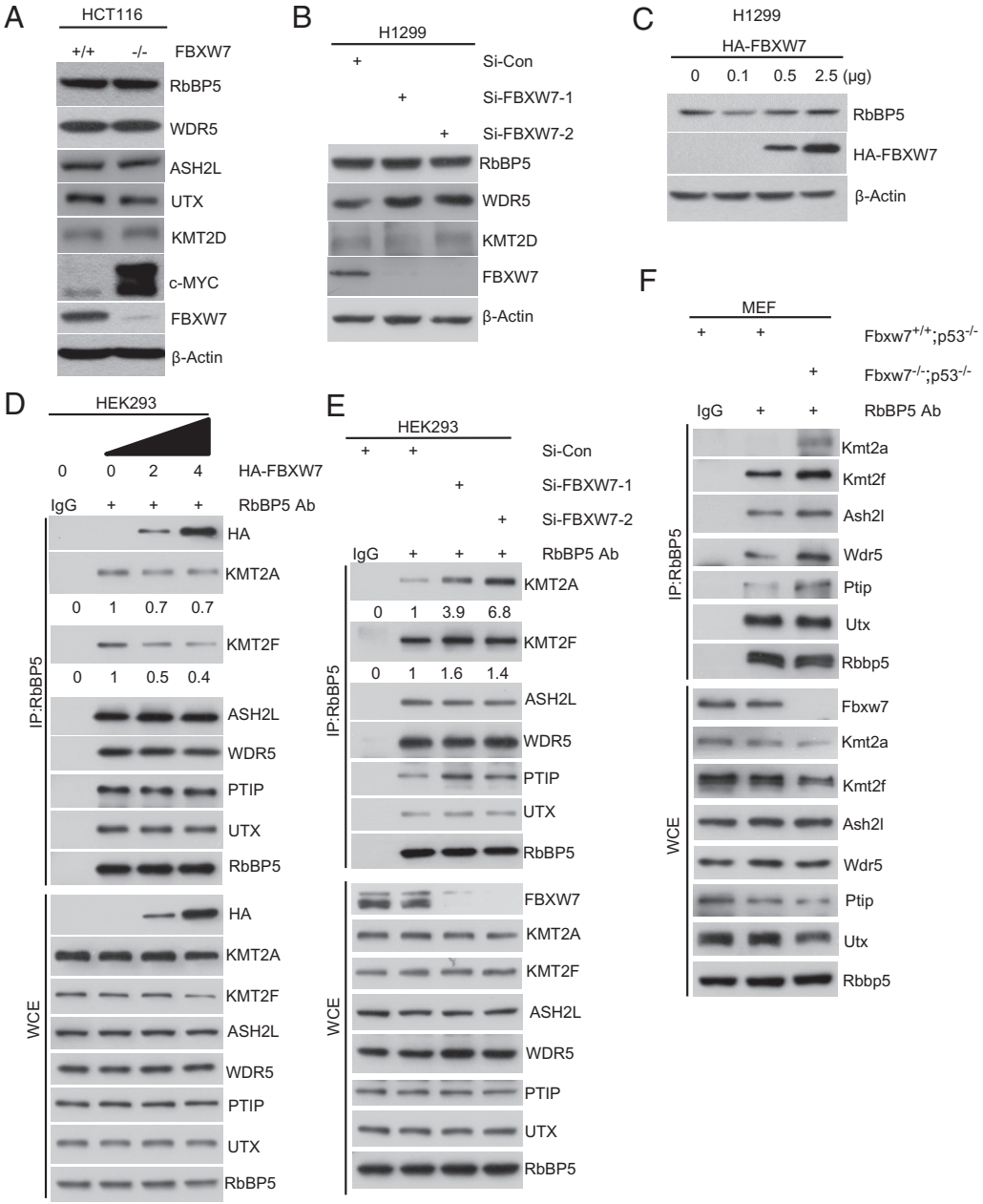


**Fig. 3.** FBXW7 does not destabilize RbBP5, but competitively inhibits RbBP5 binding to the KMT2 complexes. (*A*) HCT116 cells with or without *FBXW7* deletion were harvested for IB analysis. (*B*) H1299 cells were transfected with indicated siRNA, followed by IB analysis. (*C*) H1299 cells were transfected with the indicated amounts of HA-FBXW7, followed by IB analysis. (*D*) HEK293 cells were transfected with indicated amounts of HA-FBXW7 for 48 h, followed by IP with RbBP5 Ab and IB. (*E* and *F*) HEK293 cells were transfected with indicated siRNA for 48 h (*E*). Paired MEFs (*Fbxw7*$^{+/+}$*; p53*$^{fl/fl}$ and *Fbxw7*$^{fl/fl}$*; p53*$^{fl/fl}$) were infected with adenovirus expressing Cre recombinase (Ad-Cre) for 72 h (*F*). Cells were then harvested for IP with RbBP5 Ab, followed by IB analysis.

H3K4 methylation, we isolated MEFs from *Fbxw7*$^{fl/fl}$*;p53*$^{fl/fl}$ *or* *Fbxw7*$^{+/+}$*;p53*$^{fl/fl}$ mice. Infection with adenovirus-mediated Cre recombinase (Ad-Cre) induced the expected depletion of either p53 or both Fbxw7 and p53, compared with the Ad-GFP control (Fig. 4*D* and *SI Appendix*, Fig. S4*C*). We found that p53 depletion had no effect on H3K4 methylation, whereas Fbxw7 and p53 double depletion, similar to Fbxw7 single depletion, significantly increased H3K4 methylation (Fig. 4*D* and *SI Appendix*, Fig. S4*C*).

Given FBXW7 is frequently mutated in human cancer (32), we next determined whether several cancer-derived FBXW7 mutants would affect RbBP5 binding and H3K4 methylations. We transfected FBXW7-null HCT116 cells with plasmids encoding FBXW7-WT and three cancer-derived mutants (R465H, R479Q, R505C) individually, and found that all three mutants bind to RbBP5 with minor, if any, difference from FBXW7-WT. Furthermore, like FBXW7-WT, all these mutants inhibited H3K4 methylations as well with minor difference, consistent with their similar RbBP5 binding activity (*SI Appendix*, Fig. S4*D*).

To determine whether enhanced H3K4 methylation as a result of FBXW7 depletion was due to its regulation of KMT2 methyltransferase activity, we first used MM-102, a peptidomimetic compound that disrupts KMT2–WDR5 binding (33), thus inhibiting KMT2A (34). The treatment of paired HCT116 or MEFs with MM-102, along with DMSO as a negative control, partially blocked H3K4 methylation induced by FBXW7 deletion (Fig. 4 *E* and *F*). The same result was obtained with KMT2A knockdown in HCT116 cells (*SI Appendix*, Fig. S4*E*). Furthermore, enhanced H3K4 methylation upon FBXW7 deletion was reduced after the knockdown of either RbBP5 or KMT2F in HCT116 cells (Fig. 4*G* and *SI Appendix*, Fig. S4*F*).

To further exclude the possible involvement of KMT2D, which has been reported to be a substrate of FBXW7 in diffuse large B cell lymphoma cells (30), we crossed Fbxw7$^{fl/+}$ with Kmt2d$^{fl/+}$ mice to generate double heterozygous mice. Intercrossing of double heterozygous mice gave rise to littermate embryos with four genotypes (*Fbxw7*$^{+/+}$*;Kmt2d*$^{+/+}$, *Fbxw7*$^{fl/fl}$*;Kmt2d*$^{+/+}$, *Fbxw7*$^{+/+}$*;Kmt2d*$^{fl/fl}$, *or* *Fbxw7*$^{fl/fl}$*;Kmt2d*$^{fl/fl}$). MEFs were generated from these embryos,

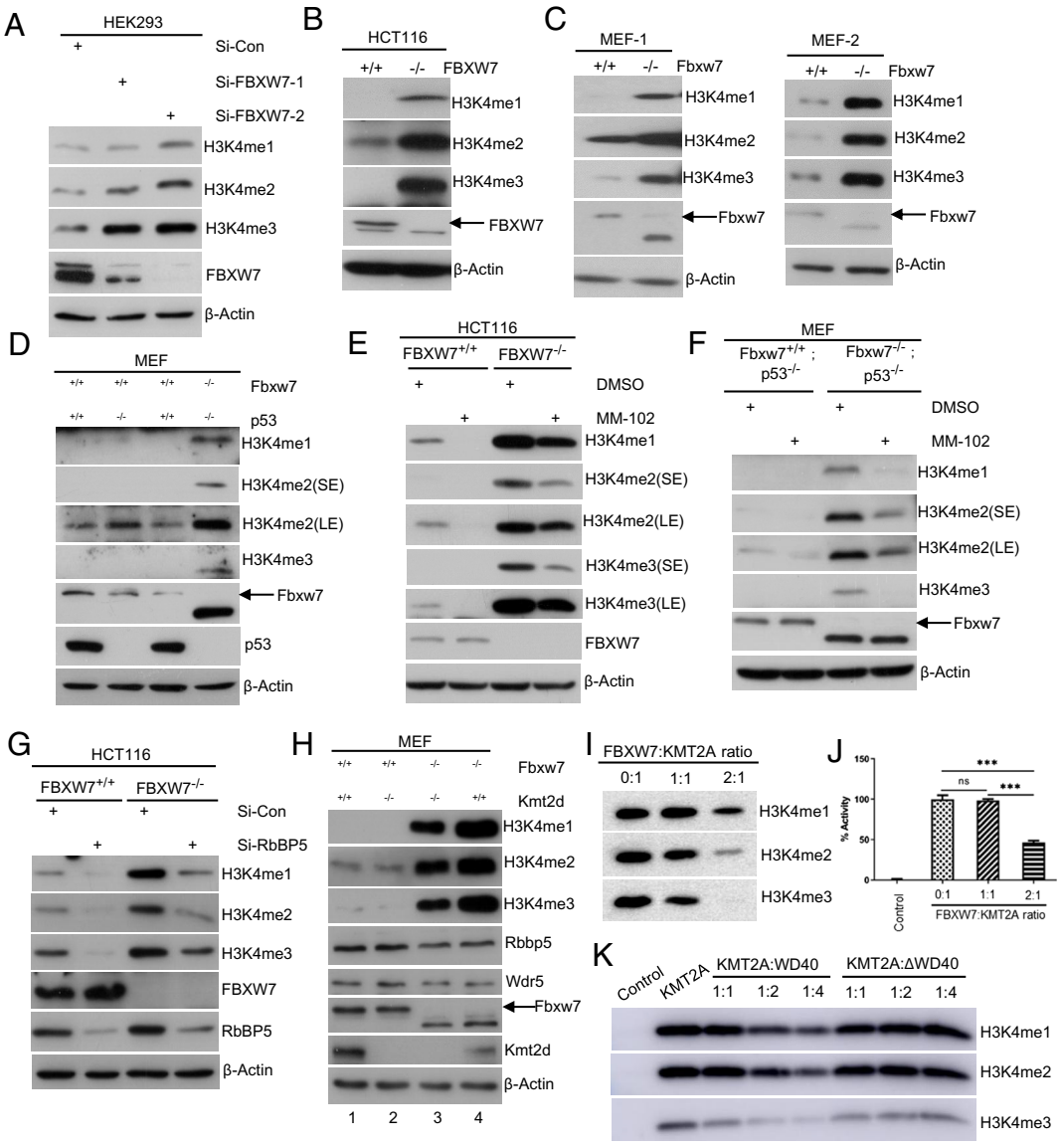


**Fig. 4.** FBXW7 inhibits KMT2 methyltransferase activity. (*A*) HEK293 cells were transfected with indicated siRNA for 48 h, followed by IB analysis. (*B* and *C*) HCT116 cells with or without *FBXW7* deletion (*B*) or two independent *Fbxw7*$^{fl/fl}$ MEFs infected with Ad-Cre or Ad-GFP for 72 h (*C*) were harvested for IB analysis. (*D*) *Fbxw7*$^{+/+}$; *p53*$^{fl/fl}$ and *Fbxw7*$^{fl/fl}$; *p53*$^{fl/fl}$ MEFs were infected with Ad-Cre or Ad-GFP for 72 h and then subjected to IB analysis. (*E* and *F*) Paired HCT116 (*E*) or MEFs (*F*) with or without *FBXW7* deletion were treated with DMSO or MM-102 at 40 μM for 72 h, followed by IB analysis. (*G*) Paired HCT116 cells were transfected with indicated siRNA for 72 h, followed by IB analysis. (*H*) *Fbxw7*$^{+/+}$; *Kmt2d*$^{+/+}$, *Fbxw7*$^{fl/fl}$; *Kmt2d*$^{fl/fl}$, *Fbxw7*$^{+/+}$; *Kmt2d*$^{fl/fl}$ and *Fbxw7*$^{fl/fl}$; *Kmt2d*$^{+/+}$ MEFs from the embryos of the same pregnant mouse were infected with Ad-Cre to delete *Fbxw7* and/or *Kmt2d* as indicated, followed by IB analysis. (*I* and *J*) The purified KMT2A and FBXW7 proteins were added into histone methyltransferase (HMT) reaction system at the indicated molar ratios, together with NCP as the substrate and SAM as the methyl source, followed by IB for H3K4 methylations (*I*) or in vitro HMT assay (*J*). KMT2A is a complex of KMT2A$_{WIN\text{-}SET}$ (3,754 to 3,969 aa), RbBP5, ASH2L, WDR5, and DPY30. n = 3; mean ± SD, ns: no significance, ***$P$ < 0.001. (*K*) The purified KMT2A and two FBXW7 truncated mutants were added into the HMT reaction system at the indicated molar ratios, followed by IB for H3K4 methylations.

followed by Ad-Cre infection to delete *Fbxw7, Kmt2d* alone or in combination. Characterization of these MEFs revealed the followings: A) *Kmt2d* deletion caused minor, if any, reduction of H3K4 methylation levels (Fig. 4*H*, lanes 1 vs. 2), whereas *Fbxw7* deletion caused robust increase of H3K4 methylation levels (Fig. 4*H*, lanes 1 vs. 4), indicating that in MEFs, *Kmt2d* plays a minimal role, whereas Fbxw7 plays a major role, in regulation of H3K4 methylations; B) the levels of H3K4 methylations were lower in *Fbxw7-Kmt2d* double knockout than *Fbxw7* single knockout (Fig. 4*H*, lanes 3 vs. 4), indicating Kmt2d indeed plays a role, although minor, in promoting H3K4 methylations; C) *Fbxw7* knockout also led to accumulation of H3K4 methylations in the absence of *Kmt2d* (Fig. 4*H*, lanes 2 vs. 3), indicating Fbxw7 regulates H3K4 methylations independently of Kmt2d; D) *Fbxw7* deletion did not cause accumulation of Kmt2d (even reducing it), nor Wdr5 and Rbbp5 (Fig. 4*H*), indicating these proteins are not Fbxw7 substrates in MEFs. Taken together, it appears that Fbxw7 is a strong regulator of H3K4 methylation independent of Kmt2d in MEFs under our experimental conditions.

Finally, we performed two independent in vitro enzymatic activity assays using the purified proteins to directly examine the inhibitory effect of FBXW7 on KMT2. We purified the core components of KMT2 complex and FBXW7 protein (*SI Appendix*, Fig. S4*G*) and performed an in vitro histone methyltransferase (HMT) assay using nucleosome core particles (NCP) as the substrate. FBXW7 inhibited H3K4 methylation by KMT2A in a dose-dependent manner, as shown by western blotting (Fig. 4*I*), and inhibited the enzymatic activity of KMT2 (Fig. 4*J*). Given either FBXW7-WD40 or FBXW7-ΔWD40 domain binds to RbBP5, we purified these truncation mutants, along with the KMT2 components (*SI Appendix*, Fig. S4*H*), and performed the same HMT assay. The results showed that only FBXW7-WD40, but not FBXW7-ΔWD40, inhibited H3K4 methylation (Fig. 4*K*). Collectively, FBXW7 inhibits KMT2 methyltransferase activity in a manner dependent on its WD40 domain.

**FBXW7 Depletion Alters Global Gene Expression via Enhanced H3K4 Methylation.** KMT2 methyltransferases are important epigenetic regulators of gene transcription that mediate histone H3K4 methylation at important regulatory regions, such as promoters and enhancers. Next, we determined whether and how FBXW7 regulates gene expression via binding with RbBP5 to inhibit KMT2, using two assays: 1) Cleavage Under Targets and Release Using Nuclease assay (CUT&RUN) assay with H3K4me1 and H3K4me3 antibodies for pull-down; 2) RNA-sequencing (RNA-seq) in a pair of MEFs with or without Fbxw7. In the CUT&RUN assay, we identified ~40,000 differential H3K4me1

peaks and ~20,000 differential H3K4me3 peaks in the whole genome (Fig. 5*A*). Overall, Fbxw7 depletion caused a remarkable increase in the up peaks, particularly in the H3K4me3 pulldown samples (Fig. 5*A*). RNA-seq profiling of triplicate samples identified more than 1,200 differentially expressed genes (DEGs) between wt and Fbxw7-depleted MEFs with the cut-off criteria of at least twofold changes and statistically significant differences (q value < 0.01). The data are summarized in a volcano plot with the red dots representing the upregulated genes and the blue dots representing the downregulated genes upon Fbxw7 depletion (Fig. 5 *B* and *C*).

We then overlapped the candidate genes identified by CUT&RUN and RNA-seq and grouped the common candidate genes into four quadrants (Fig. 5*D*). We focused on the genes in the upper right quadrant (orange part), representing 1) the genes that were enriched with more H3K4me1 or H3K4me3 at the promoter or enhancer regions, respectively, and 2) at least twofold increased mRNA levels upon Fbxw7 depletion (Fig. 5*D*), and performed Kyoto Encyclopedia of Genes and Genomes (KEGG) enrichment pathway analysis (Fig. 5*E*). Genes involved in these pathways are listed, respectively (*SI Appendix*, Fig. S5*A*).

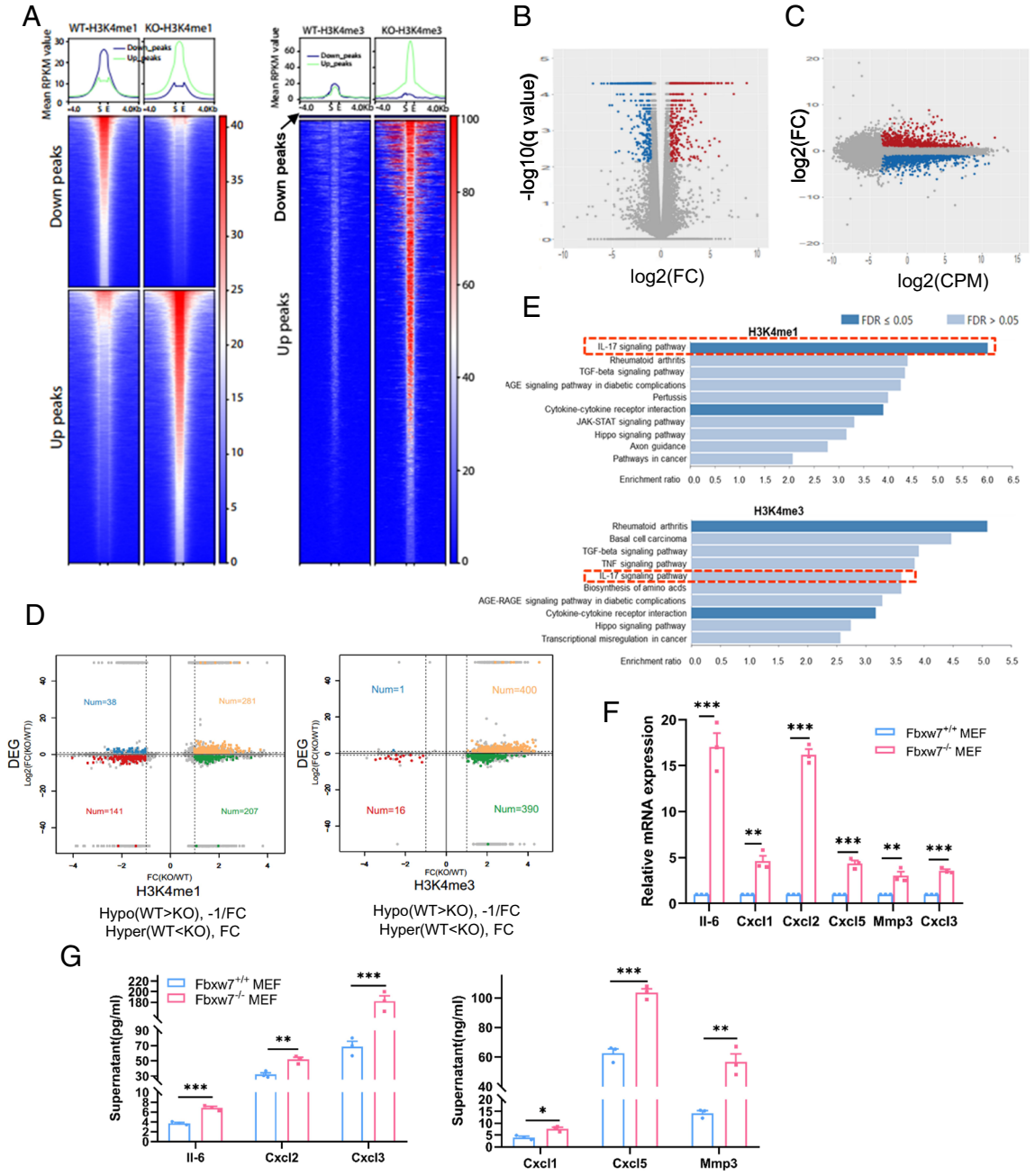


**Fig. 5.** FBXW7 depletion alters global gene expression via enhanced H3K4 methylation. (*A*) CUT & RUN assays in paired MEFs with or without *Fbxw7* deletion. The heatmaps show H3K4me1 (*Left*) and H3K4me3 (*Right*) peaks in the whole genome of paired MEFs. (*B* and *C*) RNAseq profiling in paired MEFs with or without *Fbxw7* deletion. Shown are volcano plot (*B*) and fold-change plot (*C*) for DEGs with red dots representing the up-regulated genes with at least twofold increase and the blue dots representing the down-regulated genes with a reduction of at least 50% with a q value < 0.01. FC: Fold change. (*D*) Quadrant diagrams of the overlap between DEGs from RNAseq analysis and the target genes that showed differential peaks in the promoter or enhancer regions from the CUT & RUN assay. (*E*) KEGG enrichment pathway analyses on the genes that are enriched in CUT & RUN analyses for H3K4me1 or H3K4me3 pull-down, and at least twofold increase in Fbxw7-null MEFs from RNAseq analysis, respectively. FDR: False discovery rate. (*F*) Relative expression levels of the indicated up-regulated genes from IL-17 pathway upon Fbxw7 depletion. Paired MEFs were harvested for qRT-PCR analysis. n = 3; mean ± SEM, $^{**}P < 0.01$, $^{***}P < 0.001$. (*G*) Paired MEFs were serum starved, and the supernatants were then collected as conditional media for ELISA. n = 3; mean ± SEM, $^{*}P < 0.05$, $^{**}P < 0.01$, $^{***}P < 0.001$.

Among the altered pathways, we focused on inflammatory IL-17 signaling (false discovery rate ≤ 0.05), not known to be regulated by Fbxw7. By qRT-PCR analysis, we confirmed the upregulation of these pathway genes, including IL-6, Cxcl1, Cxcl2, Cxcl5, and Mmp3, together with Cxcl3, in which H3K4me1 was enriched at its important regulatory region after Fbxw7 depletion (Fig. 5*F*), and by the CUT&RUN assay with great enrichment at the promoter or enhancer regions of these genes (*SI Appendix*, Fig. S5 *B–F*). Given that these cytokines are secreted proteins, we starved the cells and collected conditioned media to detect the levels of these proteins by ELISA. Consistent with our qRT-PCR results, we detected elevated levels of these cytokines upon Fbxw7 depletion (Fig. 5*G*). Taken together, we conclude that Fbxw7 depletion enhances KMT2 activity, leading to a genome-wide increase of H3K4 methylation to epigenetically upregulate gene transcription, including genes involved in the IL-17 signaling pathway.

Since Fbxw7 depletion activates the IL-17 signal via enhanced H3K4 methylations, we finally determined whether ectopic expression of FBXW7 or its cancer-derived mutants would rescue such an effect. We first transfected CAFs derived from pancreatic cancer with plasmids encoding FBXW7-WT and three cancer-derived mutants individually. Compared to FBXW7-WT, the mutant FBXW7-R479Q was the least effective in blocking H3K4 methylations among three mutants (*SI Appendix*, Fig. S5*G*). Consistently, this mutant was the least effective in inhibiting expression of the IL-17 signal components, including IL-6 and CXCL1/2/3/5 (*SI Appendix*, Fig. S5*H*). We then performed the rescue experiment in CAFs by simultaneously knocking down endogenous FBXW7 and ectopically overexpressing FBXW7-WT or FBXW7-R479Q, respectively. FBXW7-WT blocked upregulation of IL-6 and CXCL1/2/3/5 caused by FBXW7 knockdown, whereas FBXW7-R479Q had largely no effect (*SI Appendix*, Fig. S5*I*), suggesting a direct link between inhibition of KMT2 activity and inactivation of the IL-17 signal.

**Fbxw7 Depletion Activates the IL-17 Signaling Pathway to Promote In Vitro Migration/Invasion and Sphere Formation and In Vivo Tumor Growth upon Co-implantation of MEFs with Lung Cancer Cells.** We next determined whether the activation of IL-17 signaling pathway and its biological consequences are dependent on KMT2A activation. To prevent spontaneous senescence of primary MEFs, we used paired MEFs ($Fbxw7^{+/+}$ vs. $Fbxw7^{-/-}$) in a *p53*-null background, given that p53 had no effect on H3K4 methylation (Fig. 4*D* and *SI Appendix*, Fig. S4*C*). Since the secretory nature of IL-6, CXCL1, CXCL2, CXCL3, CXCL5, and MMP3, we cultured MEFs in serum-free medium in the presence or absence of the KMT2A inhibitor MM-102 for 72 h. We harvested the cells to measure the mRNA levels of IL-17 signaling pathway cytokines and collected the conditioned media for biological assays. MM-102 effectively blocked the induction of these cytokine mRNAs (Fig. 6*A*). Thus, cytokine induction by Fbxw7 depletion is dependent on KMT2A activity.

We then performed the Transwell assay to assess the biological effects of Fbxw7 depletion on the migration and invasion of cancer cells. Strikingly, the conditioned media collected from Fbxw7-depleted MEFs significantly promoted the migration and invasion of A549 human lung cancer cells (*SI Appendix*, Fig. S6*A*) and 4T1 murine mammary tumor cells (*SI Appendix*, Fig. S6*B*), which was largely rescued by MM-102 treatment (Fig. 6*B* and *SI Appendix*, Fig. S6*C*). Furthermore, conditioned media from $Fbxw7^{-/-}$ MEFs also stimulated sphere formation, as evidenced by the increased number and enlarged size of spheroids, which were again largely blocked/rescued by MM-102 treatment (Fig. 6*C* and *SI Appendix*, Fig. S6*D*). Collectively, we conclude from these results that Fbxw7 depletion activates IL-17 signaling pathway, along with other inflammatory pathways, to promote migration, invasion, and sphere formation of cancer cells in a manner largely dependent on KMT2A methyltransferase activity in these in vitro cell culture models.

It is well established that the TME promotes tumorigenesis and development, while CAFs are one of the primary stromal cells in the TME that participate in tumor progression by secreting tumor-promoting factors (35). We next tested our hypothesis that Fbxw7-null MEFs may promote in vivo tumor growth by secreting inflammatory cytokines/chemokines. To this end, we subcutaneously coinjected A549 lung cancer cells with $Fbxw7^{-/-};p53^{-/-}$ MEFs (right flanks) or $Fbxw7^{+/+};p53^{-/-}$ control MEFs (left flanks) at a ratio of 1:1 or 1:3, respectively, into the same immunodeficient SCID mice. While the three cell lines had comparable growth rates in the cell culture setting (*SI Appendix*, Fig. S6*E*), the in vivo growth of co-injected cells was surprisingly faster, with larger masses in $Fbxw7^{+/+};p53^{-/-}$ control group (left flanks) than in $Fbxw7^{-/-};p53^{-/-}$ group (right flanks) (Fig. 6*D* and *SI Appendix*, Fig. S6 *F* and *G*). To determine the cellular origins of "tumor" masses, we first confirmed that α-smooth muscle actin (α-SMA) can be used exclusively as a marker of MEFs with fibroblast origin, whereas cytokeratin 7 exclusively as a marker of A549 cells with epithelial origin (Fig. 6*E*). We then performed IHC staining of "tumor" masses using these two antibodies. Strikingly, while the majority of tissue masses in the $Fbxw7^{+/+};p53^{-/-}$ control group consisted of MEFs (α-SMA positive), the vast majority of the tissue masses in the $Fbxw7^{-/-};p53^{-/-}$ group were indeed tumor tissues derived from A549 cells (cytokeratin 7 positive), regardless of the ratio of the co-injection (Fig. 6*F* and *SI Appendix*, Fig. S6*H*). Consistently, the tumor tissues showed an increased proliferation rate with enhanced Ki67 staining compared to fibroblast masses, even though the latter are larger in size (Fig. 6*F* and *SI Appendix*, Fig. S6*H*). Taken together, these results demonstrate that $Fbxw7^{-/-}$ MEFs promote in vivo tumor growth by secreting more tumor-promoting cytokines/chemokines to facilitate the formation of TME. Through inactivation of KMT2 activity by RbBP5 binding, FBXW7 shows a tumor-suppressive function through a paracrine mechanism via epigenetic downregulation of inflammatory signaling pathways to block the secretion of inflammatory cytokines/chemokines.

**Hypoxia Downregulates FBXW7 via ETS1 in CAFs, Which Promotes Migration and Invasion of Cancer Cells in a Paracrine Fashion.** We next attempted to define a pathological condition analogous to that seen in our MEFs-cancer cell coinjection environment (Fig. 6*F* and *SI Appendix*, Fig. S6*H*). As mentioned earlier, FBXW7 expression in CAFs progressively decreases as disease progresses in both pancreatic and lung cancer tissues. We focused on hypoxia, which is a common condition within an outgrown tumor mass (36). We hypothesized that if FBXW7 is downregulated by hypoxia in CAFs within the TME, which could promote tumor growth in a paracrine fashion. We first cultured pancreatic ductal adenocarcinoma (PDAC-CAF) or ovarian cancer tissue (OVC-CAF) under hypoxic conditions for 24 or 48 h, and found that hypoxia indeed reduced FBXW7 protein levels, along with increased levels of H3K4 methylation with accumulation of c-JUN, a known substrate of FBXW7, as a positive control (Fig. 7*A* and *SI Appendix*, Fig. S7*A*). Similar observations of reduced Fbxw7 levels and increased H3K4 methylation were also observed in MEFs upon hypoxia exposure in a manner independent of p53 (*SI Appendix*, Fig. S7 *B* and *C*). We further found that decreased FBXW7 protein levels due to hypoxia were attributable to reduced FBXW7 mRNA expression (Fig. 7*B* and *SI Appendix*, Fig. S7*D*), suggesting that hypoxia likely induced a transcription repressor to downregulate Fbxw7 expression. The literature search revealed that 1) the transcriptional regulator

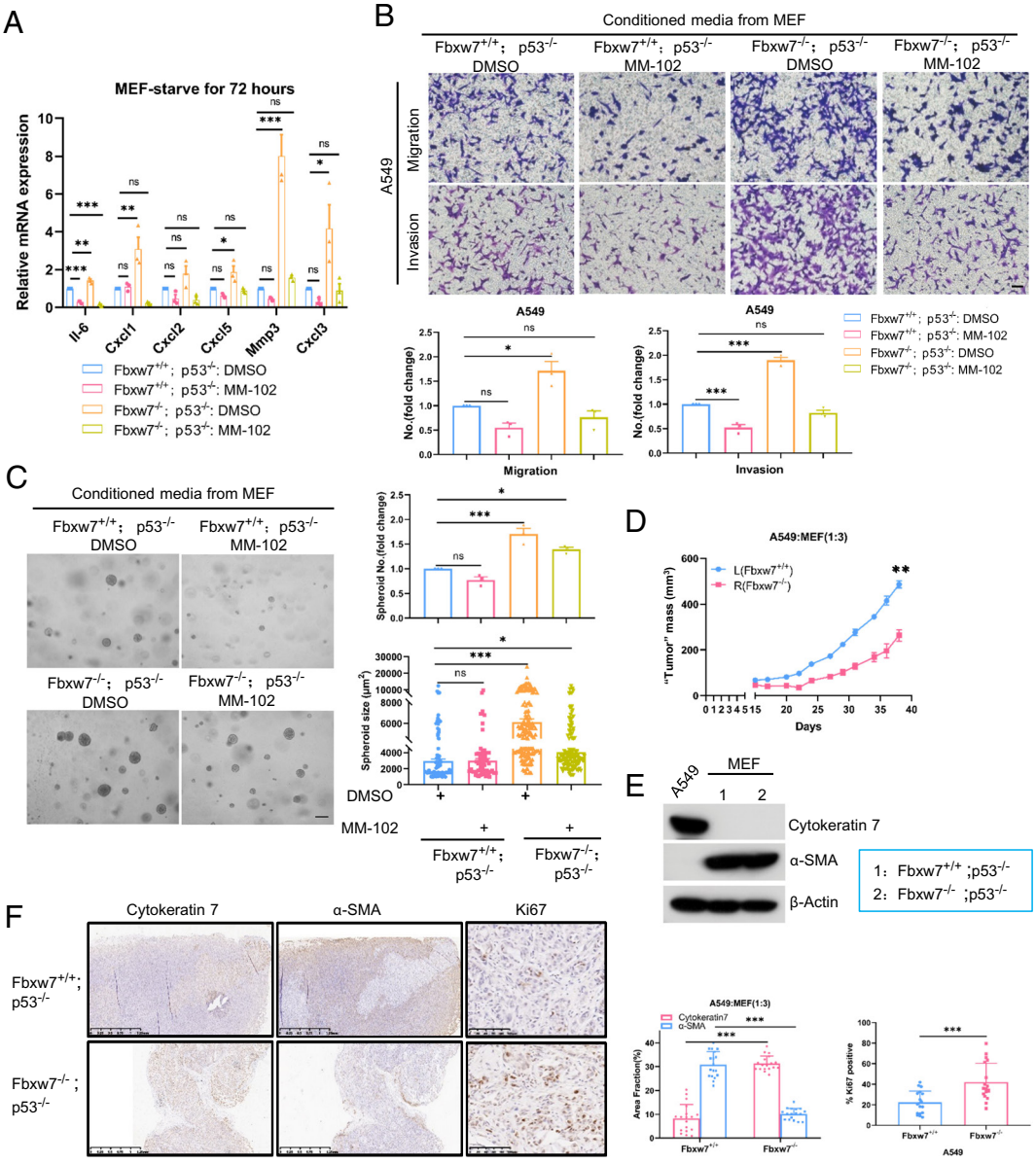


**Fig. 6.** Fbxw7 depletion activates IL-17 signaling pathway to promote in vitro migration/invasion and sphere formation and in vivo tumor growth upon co-implantation of MEFs and lung cancer cells. (*A*) MEFs with indicated genotypes were serum starved, along with MM-102 (40 μM) or DMSO treatment for 72 h, followed by qRT-PCR analysis. n = 3; mean ± SEM, ns: no significance, $*P < 0.05$, $**P < 0.01$, $***P < 0.001$. (*B*) MEFs with indicated genotypes were serum starved, along with MM-102 (40 μM) or DMSO treatment for 72 h, and then the supernatants were collected as conditioned media. 0.8 ~ 1 × $10^5$ A549 cells were seeded into the 8.0-μm, 24-well plate chamber inserts in serum-free medium, and the conditioned media were added to the wells of the plate for transwell migration and invasion assays. Shown are the representative images (*Top*) and fold changes (*Bottom*) of migrated/invaded cells. (Scale bar: 50 μm.) n = 3; mean ± SEM, ns: no significance, $*P < 0.05$, $***P < 0.001$. (*C*) Conditioned media were collected from MEFs and then mixed with DMEM containing 5% serum at a ratio of 3:1 to prepare the conditioned media dilution. A549 cells were cultured in the conditioned media dilution for 13 d under 3D culture conditions. Photographs were taken under a microscope (*Left*), and the number (expressed as fold change) and size of spheres were counted with ImageJ (*Right*). (Scale bar: 100 μm.) The difference in the spheroid numbers was expressed as fold change by setting the control group (Fbxw7$^{+/+}$p53$^{-/-}$/DMSO) as 1 (*Top Right*). For quantification of spheroid size, 58 to 145 colonies were counted (*Bottom Right*). The results were expressed as mean ± SEM from three independent experiments, ns: no significance, $*P < 0.05$, $***P < 0.001$. (*D–F*) 3 × $10^6$ A549 cells were mixed with Fbxw7$^{+/+}$; p53$^{-/-}$ or Fbxw7$^{-/-}$; p53$^{-/-}$ MEFs at a ratio of 1:3, and then s.c. injected into the left (L) or right (R) flank of SCID mice, respectively. After 15 d, the tumor volumes were measured every 2 to 3 d and the tumor growth curves were plotted (*D*). Mean ± SEM, n = 6, $**P < 0.01$. Cells were harvested for IB analysis (*E*). The subcutaneous tumors were isolated for IHC staining (*F*, *Left*). The ratios of positive staining from three random areas of each tumor (n = 6) were calculated (*F*, *Right*). Mean ± SD, n = 6, $***P < 0.001$.

CCAAT enhancer binding protein delta (C/EBPδ) was induced by hypoxia to directly inhibit FBXW7 transcription in breast cancer cells (37), and 2) the transcription repressor ETS1 was subjected to hypoxia induction, to transcriptionally repress its downstream genes (38, 39). We found that the protein levels of ETS1, but not C/EBPδ, were significantly increased in CAFs derived from both pancreatic and ovarian cancers upon hypoxic exposure (Fig. 7*A* and *SI Appendix*, Fig. S7*A*). Increased ETS1 protein was attributable to the induction of ETS1 mRNA by hypoxia, regardless of the culture conditions (Fig. 7*B*). We then focused on ETS1 and determined whether ETS1 negatively regulated FBXW7 transcription. Indeed, ETS1 knockdown increased the levels of both FBXW7 mRNA and protein in the CAFs (Fig. 7*C*). We further searched the human *FBXW7* promoter sequence and identified a consensus ETS1 binding site (AGAGGAAGTG) (40) (Fig. 7*D*). Two luciferase reporters driven by a 2-kb FBXW7 promoter sequence with or without the ETS1 binding site were constructed, and a luciferase reporter assay showed that the transcription of the FBXW7 promoter was significantly increased upon deletion of the ETS1 binding site (Fig. 7*E*). Furthermore, a chromatin IP (ChIP) assay showed direct binding of ETS1 to the FBXW7 promoter with 15-fold enrichment, as quantified by qRT-PCR (Fig. 7*F*). Importantly, similar to the observations made in MEFs, the mRNA expression of cytokines/chemokines, including IL-6 and CXCL1/2/3/5, in the IL-17 signaling pathway was also increased upon FBXW7 knockdown in CAFs (Fig. 7*G*). Taken together, these results demonstrate that in CAFs, FBXW7 is a transcription-repressing target of ETS1, which mediates hypoxia inhibition of FBXW7, and FBXW7 knockdown activates the IL-17 signaling pathway in CAFs.

Finally, we determined the biological consequences of the hypoxic repression of FBXW7 in PDAC-CAFs. We collected conditioned media from hypoxia-exposed PDAC-CAFs and found that they significantly promoted the migration and

invasion of PANC-1 and BxPC-3 pancreatic cancer cells (Fig. 7*H* and *SI Appendix*, Fig. S7*E*). Similarly, conditioned media collected from hypoxia-exposed MEFs significantly promoted the migration of A549 lung cancer cells (*SI Appendix*, Fig. S7*F*). Collectively, these results demonstrate that FBXW7 is downregulated by ETS1 at the transcriptional level in CAFs under hypoxic conditions, which in turn promotes the migration and invasion of human cancer cells in a paracrine fashion.

## Discussion

CAFs, which secrete growth factors, cytokines, and chemokines to promote cancer cell proliferation and immune exclusion, are dominant components of the TME (3). Whether and how FBXW7 regulates functions of CAFs is unknown. In this study, we found that FBXW7 serves as a tumor suppressor in CAFs, acting in a paracrine manner. Our conclusion is supported by the following lines of evidence: 1) CAF FBXW7 in TME is progressively downregulated with the advancement of human pancreatic and lung cancers; 2) FBXW7 directly binds to RbBP5, not for its ubiquitylation/degradation, but for reducing the interaction of RbBP5 with other KMT2 components, thus inactivating KMT2; 3) FBXW7 knockdown or knockout significantly increases H3K4 methylation; 4) *Fbxw7* knockout activates the IL-17 signaling pathway to secrete inflammatory cytokines and chemokines; 5) conditioned media from *Fbxw7*-knockout MEFs promotes in vitro migration and invasion and sphere formation of lung cancer cells, whereas co-injection of *Fbxw7*-knockout MEFs with lung cancer cells promotes in vivo tumor growth; 6) hypoxia exposure inhibits FBXW7 expression in CAFs derived from pancreatic

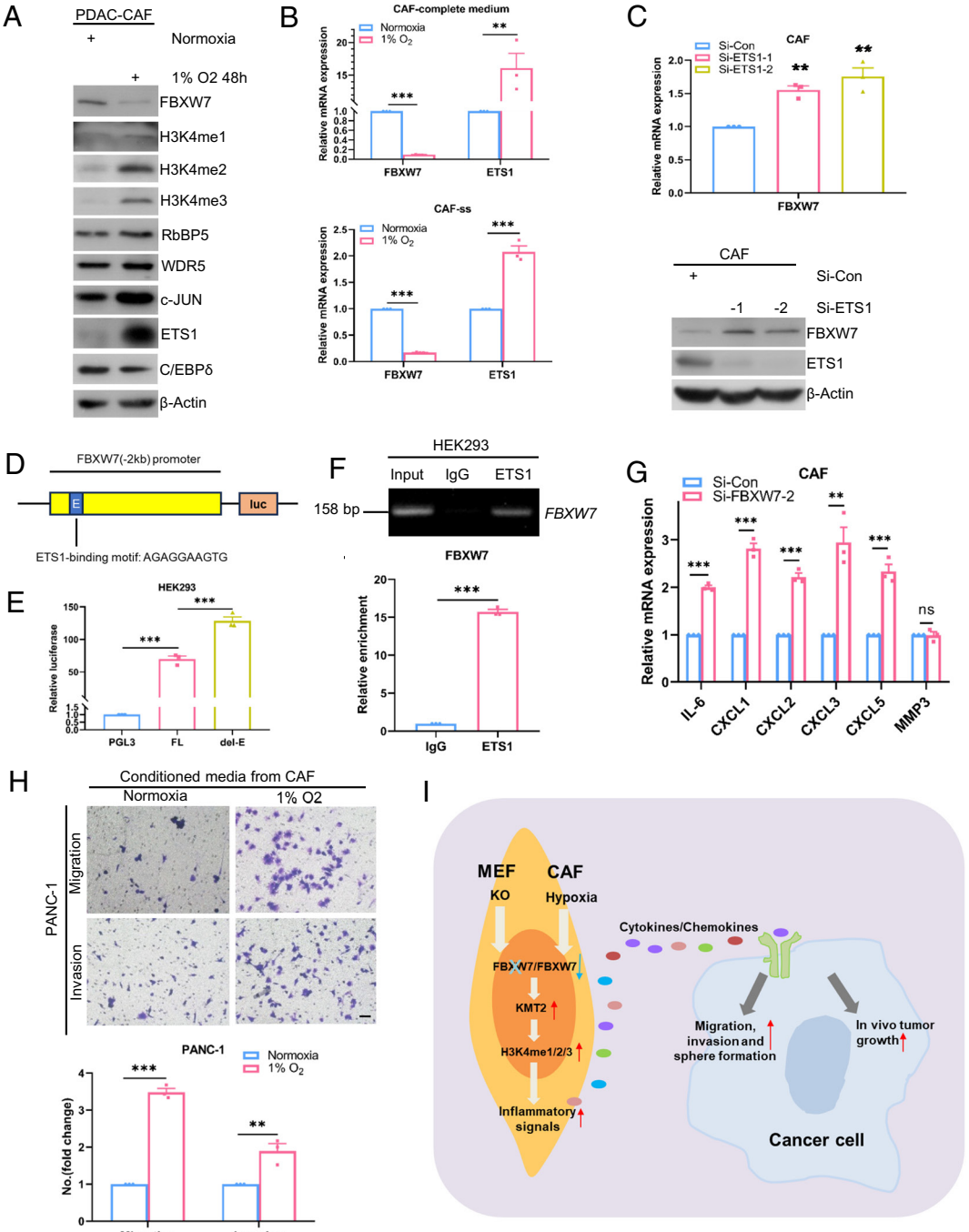


**Fig. 7.** Hypoxia downregulates FBXW7 via ETS1 in CAFs, which promotes migration and invasion of cancer cells in a paracrine fashion. (*A*) The immortalized CAFs from pancreatic cancer tissues (PDAC-CAFs) were grown under normoxia or hypoxia (1% $O_2$) for 48 h, followed by IB analysis. (*B*) PDAC-CAFs were cultured in complete (*Top*) or serum-free (*Bottom*) medium under normoxia or hypoxia for 48 h before being harvested for qPCR analysis. n = 3; mean ± SEM, $^{**}P < 0.01$, $^{***}P < 0.001$. (*C*) PDAC-CAFs were transfected with indicated siRNA for 48 h, and then cells were harvested for qRT-PCR (*Top*) or IB (*Bottom*) analysis. n = 3; mean ± SEM, $^{**}P < 0.01$. (*D*) Schematic of luciferase reporter driven by *FBXW7* promoter with ETS1 binding site indicated. E refers to ETS1 binding site. (*E*) Cells were co-transfected with luciferase reports driven by FBXW7 promoter with (FL) or without ETS1 binding site (del-E) along with Renilla, followed by luciferase reporter assay. n = 3; mean ± SEM, $^{***}P < 0.001$. (*F*) HEK293 cells were harvested for ChIP assay with ETS1 antibody, followed by PCR (*Top*) or qPCR analysis (*Bottom*). n = 3; mean ± SEM, $^{***}P < 0.001$. (*G*) PDAC-CAFs were transfected as indicated and harvested for qRT-PCR analysis. n = 3; mean ± SEM, $^{**}P < 0.01$, $^{***}P < 0.001$, ns: no significance. (*H*) PDAC-CAFs were serum starved under normoxia or hypoxia for 48 h, and then the conditioned media were collected. PANC-1 cells were seeded into the 8.0-μm, 24-well plate chamber inserts in serum-free medium, and the conditioned media were added to the wells of the plate for transwell migration and invasion assays. Shown are the representative images (*Top*), and fold changes (*Bottom*) of migrated/invaded cells. (Scale bar: 50 μm.) n = 3; mean ± SEM, $^{**}P < 0.01$, $^{***}P < 0.001$. (*I*) A working model. See text for details.

cancer tissues, whereas conditioned media from hypoxia-exposed CAFs promotes migration and invasion of pancreatic cancer cells.

We reported here that FBXW7 directly binds to RbBP5 among other five components of KMT2 complex, identified by IP-coupled mass spectrometry, in multiple human cancer cells and MEFs under the physiological condition, as well as in vitro using purified proteins. RbBP5 is known to play a pivotal role in the assembly and enzymatic activity of KMT2 family methyltransferases (34, 41, 42), and RbBP5 phosphorylation on S350 potentiates WRAD (refers to WDR5, RbBP5, ASH2L, and DPY30) assembly and regulates H3K4 methylation (43). RbBP5 also regulates the rotational dynamics of the KMT2A complex on NCPs (44, 45). Here, we showed that FBXW7–RbBP5 binding is not for degradation, but rather for blocking RbBP5 binding to other components of the KMT2 complex, leading to inhibition of KMT2 activity on mono-, di-, and tri-methylation of H3K4.

What are the biochemical consequences of FBXW7 inhibition of KMT2 activity? Given that KMT2 methylates H3K4 at the active promoter or enhancer regions in the genome (46), we performed CUT&RUN assays coupled with RNA-seq. Indeed, Fbxw7 depletion strikingly enhanced global gene expression, particularly through promoter activation, as revealed by H3K4me3 Abs-based CUT&RUN assay. KEGG analysis of genes commonly upregulated by CUT&RUN and RNA-seq revealed the activation of a few signaling pathways involved in oncogenesis and inflammation. Since the functions of CAFs within the TME are largely dependent on the secretion of soluble molecules, we focused on and confirmed the upregulation of cytokines and chemokines in the IL-17 signaling pathway in Fbxw7 depleted cells.

Previous studies have shown that FBXW7 regulates secretory proteins. For example, Fbxw7 depletion in murine BM-derived stromal cells (BMSCs) leads to Notch accumulation and consequent transcriptional activation of Ccl2, which increases Ccl2 levels in the serum, leading to the recruitment of monocytic myeloid-derived suppressor cells and macrophages, thereby promoting metastatic tumor growth (47). In addition to Ccl2, other serum chemokines such as Ccl12 and Cxcl13 were also increased after Fbxw7 depletion in BMSCs (47). In contrast, macrophage Fbxw7 promotes inflammation by ubiquitylating EZH2 for degradation to suppress H3K27me3 modification, leading to increased expression of Ccl2 and Ccl7 in a murine model of colitis (11), whereas FBXW7 in DCs also promotes inflammation by ubiquitylation and degradation of lysine N-methyltransferase suppressor of variegation 39 homolog 2 (SUV39H2) to decrease H3K9me3 modification, leading to enhanced IL-23 expression (12). Here, we show that FBXW7 epigenetically inhibits gene expression by inactivating KMT2 through RbBP5 binding. Fbxw7 depletion activates KMT2 to increase H3K4 methylation, leading to increased secretion of IL-6 and Cxcl1/2/3/5 in both MEFs and CAFs to promote migration and invasion of cancer cells in a paracrine fashion. We further extended these in vitro cell culture-based experiments to an in vivo xenograft model by co-injection of FBXW7-null MEFs with lung cancer cells into SCID mice, and confirmed that the chemokines/cytokines and other possible growth factors secreted from Fbxw7-depleted MEFs significantly stimulated the tumor growth, indicating an in vivo paracrine effect.

We also explored possible effect of cancer-derived FBXW7 mutants on RbBP5 binding and KMT2 activity. In HCT116 cells, FBXW7 mutants bind to RbBP5 and inhibit KMT2 activity equally well as FBXW7-WT. However, in CAFs derived from pancreatic cancer, a R479Q mutant was much less effective, as compared to FBXW7-WT, in blocking KMT2 activity and IL-17 signal upregulation, induced by FBXW7 knockdown. Given the fact that FBXW7 genetic mutations and deletion have opposite effect on KMT2 activity, it is unlikely that FBXW7 mutations would deliver similar effects as FBXW7 deletion via epigenetic gene regulation to influence tumorigenesis.

This study reports that FBXW7 expression is subjected to transcriptional regulation in CAFs of the TME. Starting from an in-depth analysis of published single-cell transcriptome datasets conducted in pancreatic and lung cancer tissues, we found that FBXW7 in CAFs, but not in other cell types including epithelial-origin cancer cells and various immune cells in the TME, was gradually downregulated as the disease progressed. The fact that FBXW7 expression in cancer cells of epithelial origin varies at different stages of cancer development in the TME of both pancreatic and lung cancers highly suggests that loss-of-function mutations of FBXW7 in cancer cells likely make it unnecessary for its downregulation.

What is the underlying mechanism by which CAF FBXW7 is downregulated in the TME of human pancreatic and lung cancer? It is well established that hypoxia, as one of the hallmarks of the TME, occurs frequently in a majority of human cancers when tumors outgrow the blood supply (36). Hypoxia has also been shown to promote a secretory phenotype in CAFs derived from human PDAC (48). We found that hypoxia downregulates CAF FBXW7, which is mediated by ETS1, a hypoxia-inducible transcriptional factor. We characterized FBXW7 as a transcriptional target of ETS1. It is worth noting that reduced FBXW7 mRNA expression in lung cancer tissues was also seen in other types of cells, although not progressively. Thus, it is possible the ETS1 induced by hypoxia is responsible for FBXW7 downregulation as well. Finally, we demonstrated that hypoxia biochemically downregulates FBXW7 in CAFs to increase H3K4 methylation and biologically promotes the migration and invasion of pancreatic cancer cells via a paracrine mechanism. It is well known that FBXW7 is a haploinsufficient tumor suppressor (49), and frequently mutated in human cancer, both contributing to tumorigenesis. Our finding that FBXW7 downregulation in CAFs by ETS1 under tumor hypoxic condition added one additional mechanism by which FBXW7 acts as a tumor suppressor.

In summary, our study fits the following working model: Through RbBP5 binding, FBXW7 inhibits RbBP5 interaction with other components of KMT2, leading to KMT2 inactivation. Fbxw7 depletion in MEFs or hypoxia-induced FBXW7 downregulation in CAFs activates KMT2 and increases H3K4 methylation to upregulate the expression of genes, particularly those encoding inflammatory cytokines and chemokines, in IL-17 signaling pathway. As a result, secreted cytokines/chemokines in CAFs/MEFs act in a paracrine fashion to stimulate the migration, invasion, and sphere formation of cancer cells in vitro and tumor growth in vivo (Fig. 7*I*). Thus, FBXW7 also acts as a tumor suppressor in CAFs via an epigenetic-paracrine mechanism by inactivating KMT2 activity. Our study supports therapeutic strategies targeting CAFs (3, 4), particularly those with FBXW7 downregulation, for anticancer therapy.

## Materials and Methods

The animal studies were approved by and carried out in accordance with the guiding principles of the Laboratory Animal Ethics Committee of the 2nd Affiliated Hospital of Zhejiang University School of Medicine. Immunoblotting, immunoprecipitation, half-life analysis, and hypoxia exposure were performed as previously described (50). Additional materials and methods are available in *SI Appendix, SI Materials and Methods*.

**Data, Materials, and Software Availability.** The CUT&RUN and RNA-seq data have been deposited to the NCBI GEO database (https://www.ncbi.nlm.nih.gov/geo/query/acc.cgi), and accession codes are GSE164134 (51) for CUT&RUN and GSE164135 (52) for RNA-seq. We downloaded and analyzed scRNA-seq from NCBI GEO database and accession codes are GSE205013 (25), GSE148071 (27), and GSE131907 (26). We also downloaded and analyzed scRNA-seq from gsa database (https://ngdc.cncb.ac.cn/gsa) with accession number CRA001160 (24). All study data are included in the article and/or *SI Appendix*.

**ACKNOWLEDGMENTS.** We thank Dr. Fengying Wu for her assistance with the scRNA-seq data analysis, and Dr. Zhimin Lu for stimulating discussion. This work was supported in part by the National Key R&D Program of China (2022YFC3401500 and 2021YFA1101000 to Y.S.), Zhejiang Provincial Natural Science Foundation of China (LD22H300003 to Y.S.), National Natural Science Foundation of China (82188102, 92253203, and U22A20317 to Y.S.; 81974429 and 82172898 to X.X.; and 32170656 to F.M.), and Beijing Nova Program (Z211100002121039 to F.M.).

Author affiliations: [a]Cancer Institute (Key Laboratory of Cancer Prevention and Intervention, China National Ministry of Education) of the Second Affiliated Hospital and Institute of Translational Medicine, Zhejiang University School of Medicine, Hangzhou 310009, China; [b]Institute of Medical Innovation and Research, Peking University 3rd Hospital, Beijing 100191, China; [c]Shanghai Institute of Precision Medicine, Ninth People's Hospital, Shanghai Jiao Tong University School of Medicine, Shanghai 200025, China; [d]Department of Pathology, University of Michigan, Ann Arbor, MI 48109; [e]Department of Radiation Oncology, University of Michigan, Ann Arbor, MI 48109; [f]Department of Human Genetics, University of Michigan, Ann Arbor, MI 48109; [g]Fujian Provincial Key Laboratory of Innovative Drug Target Research, School of Pharmaceutical Sciences, Xiamen University, Xiamen, Fujian 361102, China; [h]Institute of Translational Medicine, Zhejiang University School of Medicine, Hangzhou 310029, China; [i]Cancer Center of Zhejiang University, Hangzhou 310029, China; [j]Department of Gynecologic Oncology, Zhejiang Key Laboratory of Precision Diagnosis and Therapy for Major Gynecological Diseases, Women's Hospital, Zhejiang University School of Medicine, Hangzhou 310006, China; [k]Department of Medicine, University of Southern California, Los Angeles, CA 90033; [l]Department of Biochemistry and Molecular Medicine, University of Southern California, Los Angeles, CA 90033; [m]Zhejiang Provincial Clinical Research Center for CANCER, Hangzhou 310009, China; [n]Research Center for Life Science and Human Health, Binjiang Institute of Zhejiang University, Hangzhou 310053, China; and [o]Institute of Fundamental and Transdisciplinary Research, Zhejiang University, Hangzhou 310058, China

1. K. E. de Visser, J. A. Joyce, The evolving tumor microenvironment: From cancer initiation to metastatic outgrowth. *Cancer Cell* **41**, 374–403 (2023).
2. A. Dominiak, B. Chełstowska, W. Olejarz, G. Nowicka, Communication in the cancer microenvironment as a target for therapeutic interventions. *Cancers (Basel)* **12** (2020).
3. G. Biffi, D. A. Tuveson, Diversity and biology of cancer-associated fibroblasts. *Physiol. Rev.* **101**, 147–176 (2021).
4. G. Caligiuri, D. A. Tuveson, Activated fibroblasts in cancer: Perspectives and challenges. *Cancer Cell* **41**, 434–449 (2023).
5. N. Erez, M. Truitt, P. Olson, S. T. Arron, D. Hanahan, Cancer-associated fibroblasts are activated in incipient neoplasia to orchestrate tumor-promoting inflammation in an NF-kappaB-dependent manner. *Cancer Cell* **17**, 135–147 (2010).
6. K. Yumimoto, K. I. Nakayama, Recent insight into the role of FBXW7 as a tumor suppressor. *Semin. Cancer Biol.* **67**, 1–15 (2020).
7. Z. Wang, P. Liu, H. Inuzuka, W. Wei, Roles of F-box proteins in cancer. *Nat. Rev. Cancer* **14**, 233–247 (2014).
8. R. J. Davis, M. Welcker, B. E. Clurman, Tumor suppression by the Fbw7 ubiquitin ligase: Mechanisms and opportunities. *Cancer Cell* **26**, 455–464 (2014).
9. Q. Zhang *et al.*, FBXW7 facilitates nonhomologous end-joining via K63-linked polyubiquitylation of XRCC4. *Mol. Cell* **61**, 419–433 (2016).
10. H. Lan *et al.*, LSD1 destabilizes FBXW7 and abrogates FBXW7 functions independent of its demethylase activity. *Proc. Natl. Acad. Sci. U.S.A.* **116**, 12311–12320 (2019).
11. J. He *et al.*, Fbxw7 increases CCL2/7 in CX3CR1hi macrophages to promote intestinal inflammation. *J. Clin. Invest.* **129**, 3877–3893 (2019).
12. Y. Song *et al.*, Epigenetic regulation of IL-23 by E3 ligase FBXW7 in dendritic cells is critical for psoriasis-like inflammation. *J. Immunol.* **211**, 1701–1713 (2023).
13. R. C. Rao, Y. Dou, Hijacked in cancer: The KMT2 (MLL) family of methyltransferases. *Nat. Rev. Cancer* **15**, 334–346 (2015).
14. T. A. Milne *et al.*, MLL targets SET domain methyltransferase activity to Hox gene promoters. *Mol. Cell* **10**, 1107–1117 (2002).
15. Y. Dou *et al.*, Regulation of MLL1 H3K4 methyltransferase activity by its core components. *Nat. Struct. Mol. Biol.* **13**, 713–715 (2006).
16. A. Patel, V. Dharmarajan, V. E. Vought, M. S. Cosgrove, On the mechanism of multiple lysine methylation by the human mixed lineage leukemia protein-1 (MLL1) core complex. *J. Biol. Chem.* **284**, 24242–24256 (2009).
17. M. M. Steward *et al.*, Molecular regulation of H3K4 trimethylation by ASH2L, a shared subunit of MLL complexes. *Nat. Struct. Mol. Biol.* **13**, 852–854 (2006).
18. Y. Dou, J. L. Hess, Mechanisms of transcriptional regulation by MLL and its disruption in acute leukemia. *Int. J. Hematol.* **87**, 10–18 (2008).
19. J. Wysocka *et al.*, WDR5 associates with histone H3 methylated at K4 and is essential for H3 K4 methylation and vertebrate development. *Cell* **121**, 859–872 (2005).
20. D. X. Wang *et al.*, Mutation status of the KMT2 family associated with immune checkpoint inhibitors (ICIs) therapy and implicating diverse tumor microenvironments. *Mol. Cancer* **23**, 15 (2024).
21. H. Alam *et al.*, KMT2D deficiency impairs super-enhancers to confer a glycolytic vulnerability in lung cancer. *Cancer Cell* **37**, 599–617.e597 (2020).
22. E. Tinsley, P. Bredin, S. Toomey, B. T. Hennessy, S. J. Furney, KMT2C and KMT2D aberrations in breast cancer. *Trends Cancer* **10**, 519–530 (2024).
23. J. Zhu *et al.*, Gain-of-function p53 mutants co-opt chromatin pathways to drive cancer growth. *Nature* **525**, 206–211 (2015).
24. K. Chen *et al.*, Data from "Single-cell RNA-seq reveals dynamic change in tumor microenvironment during pancreatic ductal adenocarcinoma malignant progression." Genome Sequence Archive. https://ngdc.cncb.ac.cn/gsa/search?searchTerm=CRA001160. Deposited 13 October 2018.
25. G. Werba *et al.*, Data from "Single-cell RNA sequencing reveals the effects of chemotherapy on human pancreatic adenocarcinoma and its tumor microenvironment." NCBI GEO. https://www.ncbi.nlm.nih.gov/geo/query/acc.cgi?acc=GSE205013. Deposited 27 May 2022.
26. N. Kim *et al.*, Data from "Single-cell RNA sequencing demonstrates the molecular and cellular reprogramming of metastatic lung adenocarcinoma." NCBI GEO. https://www.ncbi.nlm.nih.gov/geo/query/acc.cgi?acc=GSE131907. Deposited 29 May 2019.
27. F. Wu *et al.*, Data from "Single-cell profiling of tumor heterogeneity and the microenvironment in advanced non-small cell lung cancer." NCBI GEO. https://www.ncbi.nlm.nih.gov/geo/query/acc.cgi?acc=GSE148071. Deposited 3 April 2020.
28. T. A. Soucy *et al.*, An inhibitor of NEDD8-activating enzyme as a new approach to treat cancer. *Nature* **458**, 732–736 (2009).
29. S. Hanle-Kreidler, K. T. Richter, I. Hoffmann, The SCF-FBXW7 E3 ubiquitin ligase triggers degradation of histone 3 lysine 4 methyltransferase complex component WDR5 to prevent mitotic slippage. *J. Biol. Chem.* **298**, 102703 (2022).
30. R. Saffie *et al.*, FBXW7 triggers degradation of KMT2D to favor growth of diffuse large B-cell lymphoma cells. *Cancer Res.* **80**, 2498–2511 (2020).
31. J. Han *et al.*, The internal interaction in RBBP5 regulates assembly and activity of MLL1 methyltransferase complex. *Nucleic Acids Res.* **47**, 10426–10438 (2019).
32. M. Welcker, B. E. Clurman, FBW7 ubiquitin ligase: A tumour suppressor at the crossroads of cell division, growth and differentiation. *Nat. Rev. Cancer* **8**, 83–92 (2008).
33. H. Karatas *et al.*, High-affinity, small-molecule peptidomimetic inhibitors of MLL1/WDR5 protein-protein interaction. *J. Am. Chem. Soc.* **135**, 669–682 (2013).
34. Y. Li *et al.*, Structural basis for activity regulation of MLL family methyltransferases. *Nature* **530**, 447–452 (2016).
35. L. Wang *et al.*, Cancer-associated fibroblasts contribute to cisplatin resistance by modulating ANXA3 in lung cancer cells. *Cancer Sci.* **110**, 1609–1620 (2019).
36. X. Jing *et al.*, Role of hypoxia in cancer therapy by regulating the tumor microenvironment. *Mol. Cancer* **18**, 157 (2019).
37. K. Balamurugan *et al.*, The tumour suppressor C/EBPδ inhibits FBXW7 expression and promotes mammary tumour metastasis. *Embo J.* **29**, 4106–4117 (2010).
38. S. Xing *et al.*, Hypoxia downregulated miR-4521 suppresses gastric carcinoma progression through regulation of IGF2 and FOXM1. *Mol. Cancer* **20**, 9 (2021).
39. R. Rupaimoole *et al.*, Hypoxia-mediated downregulation of miRNA biogenesis promotes tumour progression. *Nat. Commun.* **5**, 5202 (2014).
40. G. H. Wei *et al.*, Genome-wide analysis of ETS-family DNA-binding in vitro and in vivo. *Embo J.* **29**, 2147–2160 (2010).
41. Q. Qu *et al.*, Structure and conformational dynamics of a COMPASS histone H3K4 methyltransferase complex. *Cell* **174** (2018).
42. P. L. Hsu *et al.*, Crystal structure of the COMPASS H3K4 methyltransferase catalytic module. *Cell* **174** (2018).
43. P. Zhang *et al.*, A phosphorylation switch on RbBP5 regulates histone H3 Lys4 methylation. *Genes Dev.* **29**, 123–128 (2015).
44. A. Ayoub, S. H. Park, Y. T. Lee, U. S. Cho, Y. Dou, Regulation of MLL1 methyltransferase activity in two distinct nucleosome binding modes. *Biochemistry* **61**, 1–9 (2022).
45. Y. T. Lee *et al.*, Mechanism for DPY30 and ASH2L intrinsically disordered regions to modulate the MLL/SET1 activity on chromatin. *Nat. Commun.* **12**, 2953 (2021).
46. X. Zhai, J. E. Brownell, Biochemical perspectives on targeting KMT2 methyltransferases in cancer. *Trends Pharmacol. Sci.* **42**, 688–696 (2021).
47. K. Yumimoto *et al.*, F-box protein FBXW7 inhibits cancer metastasis in a non-cell-autonomous manner. *J. Clin. Invest.* **125**, 621–635 (2015).
48. S. Schwörer *et al.*, Hypoxia potentiates the inflammatory fibroblast phenotype promoted by pancreatic cancer cell-derived cytokines. *Cancer Res.* **83**, 1596–1610 (2023).
49. J. H. Mao *et al.*, Fbxw7/Cdc4 is a p53-dependent, haploinsufficient tumour suppressor gene. *Nature* **432**, 775–779 (2004).
50. L. Yin, J. Zhang, Y. Sun, Early growth response-1 is a new substrate of the GSK3β-FBXW7 axis. *Neoplasia* **34**, 100839 (2022).
51. L. Yin *et al.*, Data from "The FBXW7-KMT2 axis in cancer-associated fibroblasts controls tumor growth via an epigenetic-paracrine mechanism." NCBI GEO. https://www.ncbi.nlm.nih.gov/geo/query/acc.cgi?acc=GSE164134. Deposited 1 January 2021.
52. L. Yin *et al.*, Data from "The FBXW7-KMT2 axis in cancer-associated fibroblasts controls tumor growth via an epigenetic-paracrine mechanism." NCBI GEO. https://www.ncbi.nlm.nih.gov/geo/query/acc.cgi?acc=GSE164135. Deposited 1 January 2021.